

Article

Microstructural Evolution of Calcium Sulfoaluminate Cement during the Wet-Carbonation Process

Yangyang Zhang^{1,2,3}, Hang Yang², Qunli Zhang², Quan Qian³, Chengwei Zhang³, Kai Wu^{4,*}
and Peiliang Shen^{5,*} 

¹ State Key Laboratory of Metastable Materials Science and Technology, Yanshan University, Qinhuangdao 066004, China; yangyangzhang@ysu.edu.cn

² Hebei Province Engineering Research Center for Harmless Synergistic Treatment and Recycling of Municipal Solid Waste, Yanshan University, Qinhuangdao 066004, China; yanghangoo@stumail.ysu.edu.cn (H.Y.); zhangqunli@stumail.ysu.edu.cn (Q.Z.)

³ Hebei High Performance Building Material Technology Innovation Center, Qinhuangdao Municipal Building Materials Group Co., Ltd., Qinhuangdao 066000, China; qhdjcc@126.com (Q.Q.); zhangchengwei1992@outlook.com (C.Z.)

⁴ Key Laboratory of Advanced Civil Engineering Materials of Ministry of Education, School of Materials Science and Engineering, Tongji University, Shanghai 201804, China

⁵ Department of Civil and Environmental Engineering, The Hong Kong Polytechnic University, Hung Hom, Kowloon, Hong Kong, China

* Correspondence: wukai@tongji.edu.cn (K.W.); peiliang.shen@polyu.edu.hk (P.S.)

Abstract: Calcium sulfoaluminate (CSA) cement, as a type of low-carbon cement, can contribute to further reduction in carbon emissions with carbonation technologies. However, the detailed microstructure development of CSA cement during the carbonation process has been rarely analyzed. In this paper, wet carbonation was applied to CSA cement to investigate the microstructure evolution of carbonation products and carbon absorption capacity of CSA cement by means of pH measurement, X-ray diffraction (XRD) measurement, thermogravimetric (TG) measurement, Fourier-transformed infrared spectroscopy (FT-IR) measurement and scanning electron microscope measurement. During the carbonation process, the formed ettringite product and the dicalcium silicate clinker were carbonated immediately to generate calcium carbonate crystals, silica gel and aluminum hydroxide (AH₃) gel. With the trend of pH increasing first and notably decreasing later, the coupling interaction between the hydration and carbonation reactions of CSA cement was revealed. From the XRD and TG results, three types of calcium carbonate crystal forms (calcite, vaterite and aragonite) were detected, and the content of calcium carbonate increased with the increase in carbonation time. FT-IR analysis further confirmed the existence of calcium carbonate, silica gel and AH₃ gel with their characteristic vibrations. Moreover, the microstructure of carbonation products with different morphologies was observed. The application of wet carbonation to CSA cement provides a more comprehensive insight to the carbonation mechanism of this low-carbon cement.

Keywords: calcium sulfoaluminate cement; carbonation; microstructure; thermodynamic modeling



Citation: Zhang, Y.; Yang, H.; Zhang, Q.; Qian, Q.; Zhang, C.; Wu, K.; Shen, P. Microstructural Evolution of Calcium Sulfoaluminate Cement during the Wet-Carbonation Process. *Buildings* **2024**, *14*, 343. <https://doi.org/10.3390/buildings14020343>

Academic Editors: Denny Coffetti and Chuang Feng

Received: 30 November 2023

Revised: 15 January 2024

Accepted: 24 January 2024

Published: 26 January 2024



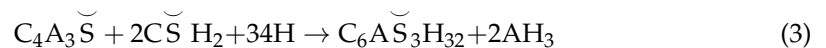
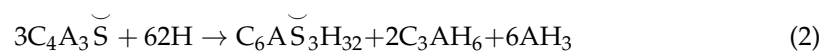
Copyright: © 2024 by the authors. Licensee MDPI, Basel, Switzerland. This article is an open access article distributed under the terms and conditions of the Creative Commons Attribution (CC BY) license (<https://creativecommons.org/licenses/by/4.0/>).

1. Introduction

Nowadays, the annual production of Portland cement in China is approximately 2.4 billion tons, ranking first in the world. However, approximately 0.9 t CO₂ is released during the production of 1t Portland cement, making the cement industry an important source of carbon emissions [1–3]. It is reported that the carbon emissions of the Portland cement industry around the world have accounted for approximately 26% of the total industrial carbon emissions and approximately 7% of the total human carbon emissions. Therefore, in order to achieve China's strategic goals of "carbon neutrality and peak carbon emissions", it is urgent to reduce carbon emissions from the cement industry [4]. Carbon capture, utilization and storage (CCUS) technology has been proposed recently to prevent

excessive carbon emissions, which includes three main processes: CO₂ capture, utilization and storage. CO₂ capture is the separation and collection of CO₂ from factory emission sources; CO₂ utilization refers to the use of captured CO₂ for the manufacture of new products; CO₂ storage is the storage of captured CO₂ underground [5,6]. Researchers are constantly exploring better applications of CCUS technology in the cement and concrete industry [7,8].

Calcium sulfoaluminate cement (CSA cement), as the third series of cement independently developed in China, has become a highly promising low-carbon cement due to its advantages of low calcination temperature, low consumption of limestone as raw materials and easy wear resistance [9–12]. In addition, CSA cement has high early strength, good impermeability and frost resistance and micro-expansion characteristics. It has also been successfully applied in emergency repair and construction, marine construction and other projects [4,13,14]. Ye’elite (C₄A₃S̄) and belite (C₂S) are the main minerals in CSA cement: The former enables this type of cement to have quick hardening speed and early strength on account of its rapid hydration, and the latter provides later strength owing to the C-S-H gel generated at the later age. Generally, the hydration of C₄A₃S̄ occurs according to Equation (1) to generate monosulfate (C₄AŠH₁₂) and aluminum hydroxide (AH₃) gel. Under the circumstances of excessive water, C₃AH₆ may form according to Equation (2). Actually, during the manufacture of CSA cement, gypsum (CŠH₂) or anhydrite is used, and C₄A₃S̄ will react with calcium sulfate to generate ettringite (C₆AŠH₃₂) and AH₃ (Equation (3)). Moreover, the hydration of C₂S tends to generate C-S-H and portlandite (CH) according to Equation (4). With the hydration of C₄A₃S̄ and C₂S at the same time, C₂S will react with AH₃ to generate strätlingite (C₂ASH₈) (Equation (5)).



As for the carbonation of CSA cement, most of the studies have focused on its mechanical property, such as compressive strength, expansion, etc. [15–21]. For instance, after carbonation, the mechanical property of CSA cement was improved as reported by Mechling [22], but it was also influenced by the water-to-cement ratio. Moreover, different carbonation methods usually present various results, e.g., a carbonation chamber is usually used for carbonation, and thus, the difference between the accelerated carbonation and the environmental carbonation can be investigated. Seo [20] studied CSA cement that was supplemented with different amounts of MgO, and after hydration for 56 d, the samples were carbonated for studying compressive strength; the result showed that the optimal dosage of MgO was 10 wt.% for improvement of strength. By mixing with slag, the mechanical property of CSA cement can be promoted after being exposed to CO₂ for further carbonation [23]. Regarding the microstructure during the carbonation of CSA cement, it was found that, after ettringite was entirely carbonated, the carbonation products mainly consisted of gypsum and calcium carbonate (in three polymorphs, i.e., calcite, aragonite and vaterite), which has been found with the XRD results reported by Daniela Gastaldia [19]. Also, the carbonation of CSA cement supplemented with PC was reported, and the carbonation of monosulfate was revealed rather than ettringite, as the ettringite content was not substantially decreased, and the generation of gypsum was attributed to the carbonation of monosulfate [19]. For the carbonation of CSA cement, the sample was normally hydrated for a certain number of days (28 d or 56 d) and then put into a carbonation chamber for research. This means that the traditional carbonation method applied for CSA cement was a method of hydration followed by carbonation.

As an important carbonation method, wet carbonation has always been in the stage of continuous development and deep exploration. The contact area and dissolution rate of CO₂ can be increased with wet carbonation, which is helpful to simulate and observe the carbonation process in a short time [24]. Researchers are dedicated to studying the kinetics and thermodynamics of the interaction between cement components and CO₂ as well as the impact of different environmental conditions (temperature, humidity, pressure, etc.) on carbonation. Additionally, the mechanical properties and microstructure of cement or concrete after carbonation are evaluated. For instance, the impacts of gas pressure, water-to-solid ratio, gas-to-liquid ratio and reaction time on CO₂ absorption were assessed by introducing cement plant flue gas into discarded concrete [25]. The results indicate that increasing the total gas pressure, gas–liquid ratio and liquid–solid ratio is an effective method to enhance the efficiency of mineral carbonation. By using waste CO₂ to wet carbonated recycled concrete aggregate (RAC) and recycled concrete fine particles (RCF), the purposes of absorbing more carbon dioxide and improving the material properties would be achieved [26,27]. The wet-carbonation process was characterized in detail, revealing changes in the microstructures (such as pores and carbonation products), compressive strength and other mechanical properties. This approach demonstrates the advantages of efficient and low-energy wet carbonation. Direct carbonation of synthetic concrete powder was achieved by controlling various solid-to-liquid ratios (10, 25 and 50 g/L) and different concentrations of CO₂ (5%, 14% and 30%). Characterization involves assessing the carbonation products, CO₂ absorption capacity and crystalline structure of the resulting calcium carbonate [24].

In general, the carbonation of CSA cement was previously studied with dry carbonation or environmental carbonation, where CSA cement was hydrated first and then exposed to CO₂. Therefore, in this work, wet carbonation was applied in the carbonation of CSA cement to study the coupling mechanism of hydration and carbonation reactions, and the corresponding microstructure evolution was investigated. The wet carbonation applied in CSA cement can be revealed for guidelines of the carbonation mechanism of CSA cement. By means of XRD, TG and FT-IR, the evolution of the microscopic phases was studied, and the microstructure was displayed from SEM images. Also, thermodynamic modeling was conducted for further explanation.

2. Experimental Programs

2.1. Raw Materials and Characterization

In this work, a fast-hardening calcium sulfoaluminate cement was used. The chemical compositions of the CSA cement used in this study are as follows: 13.86 wt.% SiO₂, 24.06 wt.% Al₂O₃, 2.71 wt.% Fe₂O₃, 39.39 wt.% CaO, 2.66 wt.% MgO, 13.58 wt.% SO₃, 1.35 wt.% TiO₂ and 1.43 wt.% Loss. The cement mineral composition was obtained with Rietveld quantification on the XRD pattern (Table 1). As observed in Table 1, the CSA cement mainly consists of 38.52 wt.% ye’elimite, 24.23 wt.% belite, 20.78 wt.% anhydrite, 8.56 wt.% brownmillerite, 2.91 wt.% mayenite, 2.40 wt.% gypsum and 2.59 wt.% quartz. The particle size distribution obtained with a laser particle size analyzer (BT-9300H) is presented in Figure 1, and 90% of the particles are under 75 µm. The values of D10, D50 and D90 are 1.53 µm, 13.93 µm and 42.88 µm, respectively. The surface area of the cement is 599.3 m²/kg.

Table 1. Quantitative phase analysis results of CSA cement.

| Mineral Phase | wt.% |
|---|-------|
| Ye’elimite (C ₄ A ₃ S̄) | 38.52 |
| Belite (C ₂ S) | 24.23 |
| Anhydrite (C̄S) | 20.78 |
| Brownmillerite (C ₄ AF) | 8.56 |
| Mayenite (C ₁₂ A ₇) | 2.91 |
| Gypsum (C̄SH ₂) | 2.40 |
| Quartz (SiO ₂) | 2.59 |

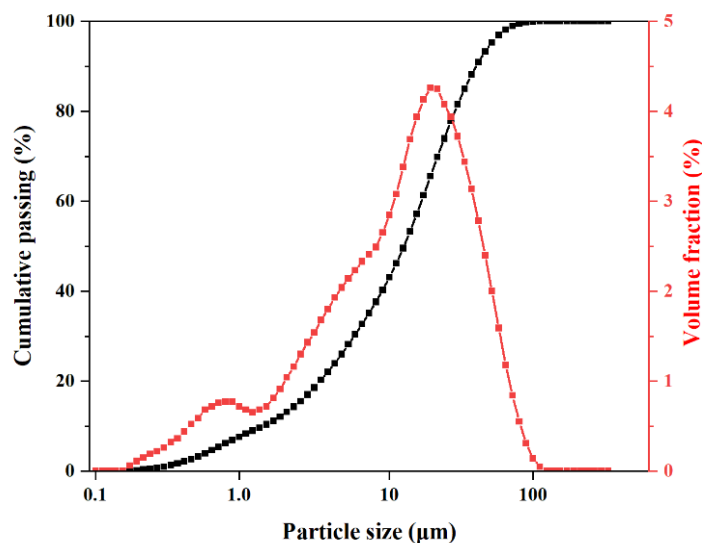


Figure 1. Particle size distribution of CSA cement.

2.2. Wet-Carbonation Process

The same batch of cement with the same particle size was used in this work. The experiment was carried out in a special reaction device, as shown in Figure 2. CSA cement and deionized water were added to the beaker with a mass ratio of 1/20 at room temperature, and the mixed paste was stirred in the beaker for 10 min for a stable pH value. The speed of stirring was constantly kept at 200 rpm. CO₂ with a 99.9% concentration was injected into the solution through a sparkling stone at a flow rate of 150 mL/min, and the pressure of CO₂ was maintained at 0.2 MPa throughout the entire process. Samples with different carbonation times of 10 s, 30 s, 1 min, 2 min, 5 min, 10 min, 15 min, 20 min, 30 min, 1 h, 2 h, 12 h and 24 h were prepared as separate batches. After a certain period of carbonation, the carbonated samples were filtered first, and isopropanol was used for the termination of both carbonation and hydration. After filtering, these samples were dried in a vacuum drier for 8 min at 40 °C [28].

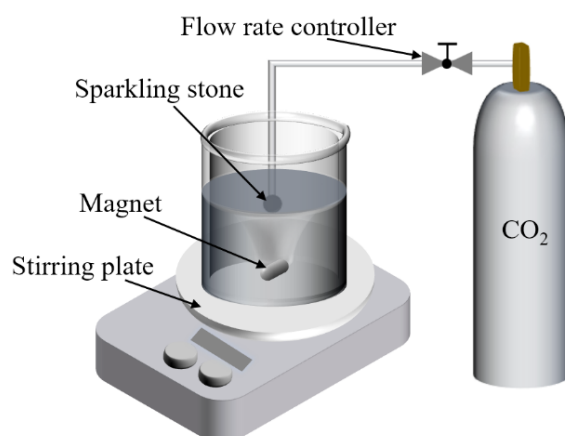


Figure 2. Schematic illustration of the wet-carbonation reaction device.

2.3. Test Methods

2.3.1. pH Measurement

All carbonated samples were filtered to obtain filter residue and solution. The pH of each filtrate was measured with a pH meter (model REX PHS-3C).

2.3.2. X-ray Diffraction (XRD) Measurement

The crystalline phase was analyzed with Rigaku SmartLab, an intelligent X-ray polycrystalline diffractometer. During the test, the working voltage was 45 kV, the working current was 200 mA, and the scanning speed was set at $2^\circ/\text{min}$ with a range of $5\text{--}80^\circ 2\theta$. ZnO as the internal standard was added to the sample for the quantitative analysis [29–32]. EVA V3.1 software was used to qualitatively analyze the XRD pattern and determine the product types. TOPAS 4.2 software was used to quantitatively analyze the XRD pattern and determine the content of each phase.

2.3.3. Thermogravimetric (TG) Measurement

The TG-DTG of the samples with different carbonation times was measured with a Hitachi Limited thermogravimetric analyzer. The test temperature ranged from 30°C to 1000°C . The heating rate was $10^\circ\text{C}/\text{min}$, and the N_2 atmosphere was kept at the speed of $40\text{ mL}/\text{min}$.

2.3.4. Fourier-Transformed Infrared Spectroscopy (FT-IR) Measurement

The FT-IR spectroscopy was conducted with a Bruker INVENIO spectrometer. The resolution of the test was 4 cm^{-1} , and the scope of the data scan was from 4000 cm^{-1} to 400 cm^{-1} . In addition, each sample went through 32 scanning times.

2.3.5. Scanning Electron Microscope (SEM) Measurement

A TESCAN Vega3 was used to observe and analyze the morphology and particle size of each sample after carbonation. The carbonated powder was applied to the carbon glue, and gold was sprayed once through the SBC-12 ion sputtering meter, keeping the current at 10 mA. The operating software Vega TC was employed for scanning and analyzing.

2.3.6. GEMS Modeling

Gibbs free-energy minimization software (GEMS V3.7) was employed to predict the formation and transformation of the different phases involved in the cement carbonation reaction. The CEMDATA18 database dedicated to cement was used in the simulation process. The final stable products of CSA cement after hydration and carbonation were simulated as a reference for the experiment.

3. Results and Discussion

3.1. pH Analysis

Figure 3 shows the pH value at the different carbonation times of 10 s, 30 s, 1 min, 2 min, 5 min, 10 min, 15 min, 20 min, 30 min, 1 h, 2 h, 12 h and 24 h, respectively. After carbonation for 30 s, the pH reached the maximum value of 10.5, which was probably linked to the hydration of CSA cement despite the addition of CO_2 . As reported before, the pH value of hydrated cement paste always ranges from 12 to 13 [33]. Although the pH value had not reached 12 at 30 s, it could be considered that the carbonic acid in the solution reduced the pH value. After carbonation for 1 min, the pH of the solution decreased rapidly, which can be attributed to the occurrence of the carbonation reaction along with the formation of carbonic acid. It is worth noting that, before 10 min, the pH of the solution was alkaline, which can be associated with the hydration of $\text{C}_4\text{A}_3\text{S}$ and C_2S , but the pH of the solution was acidic after 10 min, owing to the excessive addition of CO_2 to form carbonic acid in the solution. Ultimately, the pH value of the solution tended to be stable beginning from 10 min. Generally, after exposure to a large amount of CO_2 , the pH showed an increased trend, followed by a decreased trend, which revealed the coupling interaction between the hydration and carbonation reactions [21,34–37].

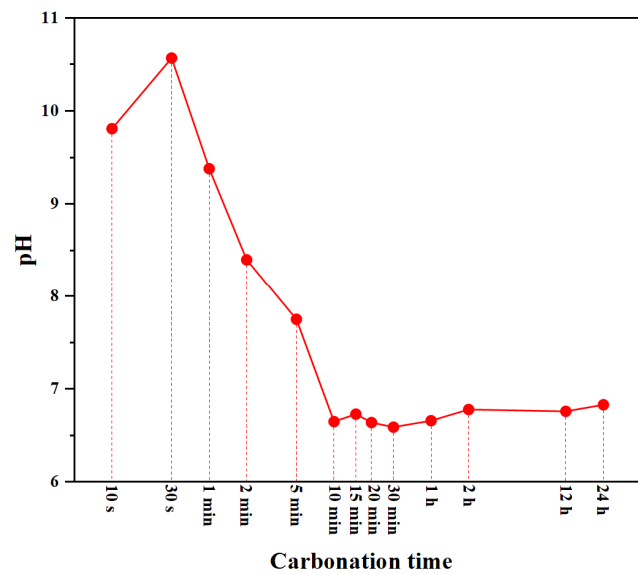


Figure 3. pH values of the solution at different carbonation times.

3.2. XRD Analysis

The XRD patterns of the carbonated samples are shown in Figure 4. The main components of CSA cement, i.e., $C_4A_3\check{S}$, C_2S and anhydrite, can be observed with the XRD diffraction peaks throughout the entire process. With the increasing carbonation time, the diffraction peaks of $C_4A_3\check{S}$ and C_2S gradually weakened. The diffraction peaks of gibbsite, one of the hydration products of $C_4A_3\check{S}$ [37], can be detected throughout the carbonation process. The diffraction peaks of ettringite were not visible, owing to its carbonation reaction. On the other hand, as the pH rapidly diminished, it was difficult for the ettringite to exist stably in this pH environment [38].

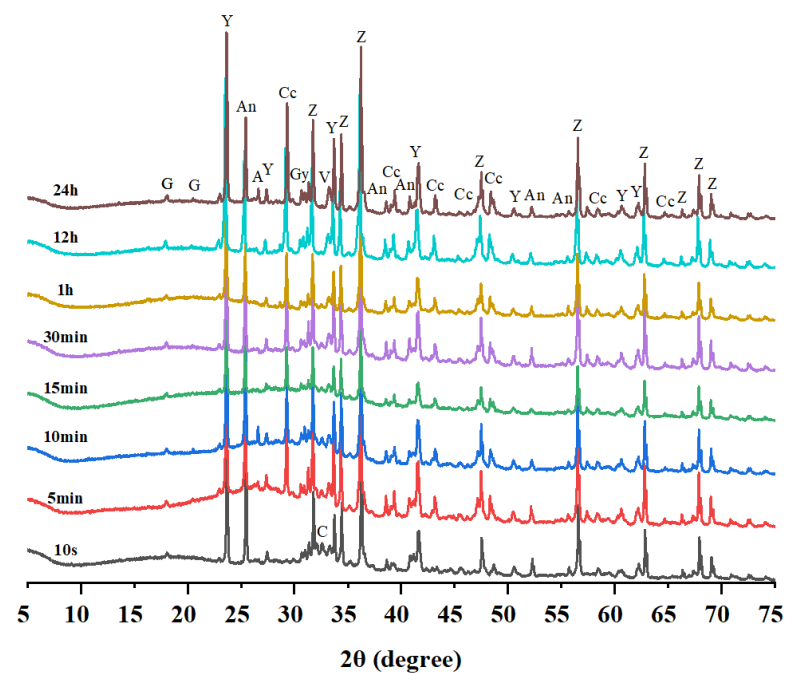


Figure 4. XRD patterns of the samples at various carbonation times. V: vaterite; Gy: gypsum; Cc: calcite; A: aragonite; Z: ZnO; An: anhydrite; G: gibbsite; Y: $C_4A_3\check{S}$; C: C_2S .

Generally, the primary distinction of the XRD diffraction peaks was calcium carbonate. After carbonation for 10 min, calcite, aragonite and vaterite began to generate, which can

be associated with the carbonation of ettringite and the hydration products of belite [39]. Regarding the samples carbonated for 10 s, there was no calcium carbonate generated, and it can be attributed to the formation of carbonic acid in the solution rather than the carbonation of ettringite or the hydration products of belite. Furthermore, after carbonation for 15 min, aragonite was no longer visible until carbonation for 24 h. It can be observed from the XRD pattern that calcite showed sharp characteristic diffraction peaks at 2θ degree of 29.2° along with diffraction peaks at 2θ degree of 39.4° , 43.2° , 48.3° and 57.5° ; vaterite showed a diffraction peak at 2θ degree of 32.5° , and aragonite showed a diffraction peak at a degree of 26.3° . In addition, the peaks of $C_4A_3\check{S}$ and anhydrite varied with the amount of CO_2 , which possibly suggested the different hydration degree of $C_4A_3\check{S}$ and anhydrite. In Table 2, the QXRD analysis of each carbonated sample acquired with Rietveld quantification is given for further explanation. Figure 5 shows an example of the Rietveld plot.

Table 2. Quantitative phase analysis results for CSA cement at various carbonation times (wt.%).

| | 10 s | 5 min | 10 min | 15 min | 30 min | 1 h | 12 h | 24 h |
|-------------------|-------|-------|--------|--------|--------|-------|-------|-------|
| $C_4A_3\check{S}$ | 33.80 | 27.36 | 24.29 | 25.54 | 26.42 | 28.64 | 28.60 | 26.99 |
| C_2S | 23.78 | 21.04 | 23.79 | 23.56 | 16.59 | 1.58 | 0.82 | 0.18 |
| Anhydrite | 13.72 | 14.95 | 14.38 | 14.38 | 11.76 | 11.31 | 10.87 | 9.69 |
| Gypsum | 5.90 | 5.97 | 5.98 | 7.04 | 5.11 | 4.42 | 5.36 | 5.92 |
| Calcite | - | 13.08 | 15.31 | 13.58 | 9.69 | 10.92 | 15.64 | 14.49 |
| Vaterite | - | 7.03 | 6.13 | 4.90 | 0.92 | 1.51 | 1.09 | 3.04 |
| Aragonite | - | 0.90 | 2.66 | - | - | - | - | 0.42 |
| Gibbsite | 3.83 | 1.90 | 0.51 | 0.21 | 5.21 | 11.00 | 3.79 | 0.77 |
| Amor. | 18.96 | 7.77 | 6.94 | 10.78 | 24.30 | 30.61 | 33.85 | 38.53 |
| R_{wp} (%) | 8.74 | 10.98 | 9.68 | 6.32 | 7.99 | 9.83 | 8.17 | 9.61 |

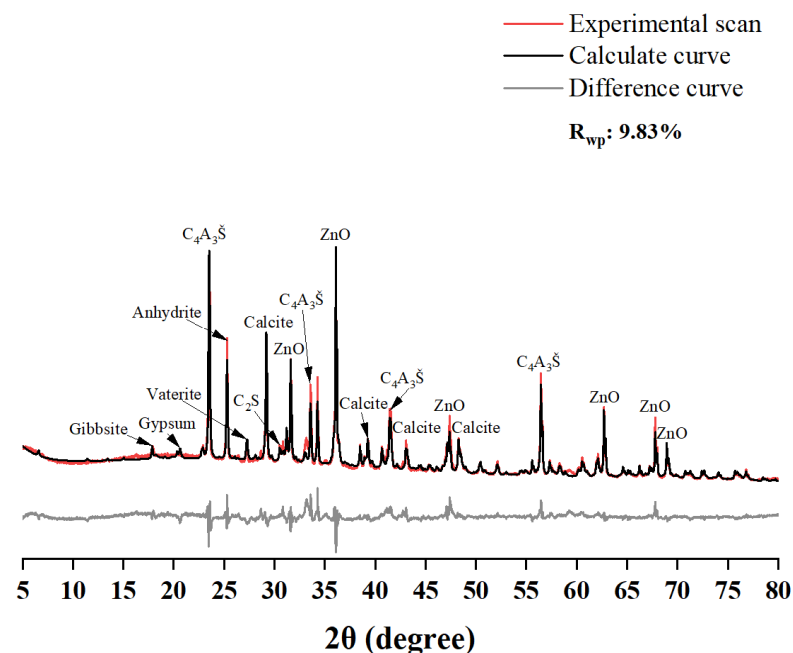


Figure 5. Rietveld plot of CSA cement carbonated for 1 h.

As observed in Table 2, the content of the two main components ($C_4A_3\check{S}$ and C_2S) decreased significantly as the carbonation time increased, and the decrease of C_2S was faster than that of $C_4A_3\check{S}$ since C_2S is more prone to carbonation as reported before [30]. The result that $C_4A_3\check{S}$ decreased before 15 min with no variation later suggested that both its hydration and carbonation occurred before 15 min, and later, the hydration of $C_4A_3\check{S}$ no longer proceeded, let alone the carbonation reaction; this result can be proved by the change in C_2S , which showed a slight decrease before 15 min and a rapid reduction later.

After 24 h of carbonation, C_2S was almost completely carbonated to generate different types of calcium carbonate. However, the decrease in $C_4A_3\check{S}$ exhibited a relatively low trend compared to C_2S , as the formation of ettringite was inhibited in the acidic environment, and thus, the hydration of $C_4A_3\check{S}$ was indirectly inhibited as well. Meanwhile, the amount of anhydrite diminished as well, which can be attributed to its hydration with $C_4A_3\check{S}$. Specifically, no ettringite was generated on account of its carbonation, and gypsum and calcium carbonate were generated as a result. Regarding the amount of gypsum, it can be concluded from Table 2 that its content reached a maximum value at 15 min and then diminished partly to the end. It can be ascribed to the presence of $C_4A_3\check{S}$ in the solution and the further reaction between $C_4A_3\check{S}$ and gypsum. In other words, the hydration of $C_4A_3\check{S}$ in the solution involved mainly two parts: One is the reaction with anhydrite, and the other is the reaction with the generated gypsum. These small amounts of gypsum reacted with $C_4A_3\check{S}$ to generate ettringite, which was immediately carbonated, and it further confirmed the carbonation of ettringite despite no obvious characteristics of ettringite in the XRD pattern.

The content of C_2S decreased with increasing carbonation time, especially for carbonation for more than 15 min, indicating the occurrence of the carbonation reaction, whose carbonation mainly leads to the generation of calcium carbonate, as is observed from the XRD results and QXRD results. Among the three types of calcium carbonate, calcite increased rapidly at the early stage of carbonation (from 10 s) and gradually stabilized in the later stage. The content of calcite reached the maximum value at 10 min. Before 15 min, vaterite existed in a large amount, but its content gradually decreased after 15 min. In addition, aragonite was not detected until 24 h, which can be observed from the XRD result at 24 h. Although each content was relatively low, vaterite and aragonite still existed until C_2S was entirely carbonated (the sample at 24 h). It is worth noting that the content of calcium carbonate also decreased slightly. In addition to calcite with good crystal form, poorly crystallized or amorphous calcium carbonate was also observed. As shown in Table 2, the amorphous content was increasing. As for gibbsite, its quantity reached the maximum value after being exposed to CO_2 for 1 h, which proved the coupling interaction between the hydration and carbonation reactions as well; and the amount of gibbsite decreased after 12 h, which was probably associated with its reaction with C_2S and the further carbonation of the formed strätlingite.

3.3. FT-IR Analysis

Figure 6 shows the FT-IR spectra of the carbonated samples at 10 s, 30 s, 1 min, 2 min, 5 min, 10 min, 15 min and 30 min. A signal O-H band positioned at 3436 cm^{-1} was visible in all of the samples, which represented the vibration frequencies characteristic of the gibbsite formed in the samples. With increasing carbonation time, the signal at 1410 cm^{-1} appeared more obvious, which was associated with C-O vibration in the calcite. In the samples carbonated for 10 s and 30 s, this signal was not observed in the spectra and further confirmed the XRD result that no calcite was generated at the earlier carbonation time. Meanwhile, the signals of C-O vibration at 875 cm^{-1} gradually sharpened with increasing carbonation time, which demonstrated the generation of calcite as well. Moreover, the C-O vibration located at various peaks represents the different morphologies of calcium carbonate, e.g., vibrations at 713 cm^{-1} and 745 cm^{-1} stand for the presence of aragonite and vaterite. Therefore, after being exposed to CO_2 , aragonite and vaterite were generated, owing to their characteristic peaks at the FT-IR spectra. In addition, Si-O vibration at 510 cm^{-1} was the characteristic peak of C_2S , and its intensity began to weaken as the carbonation time prolonged, which further proved its carbonation as a result of calcium carbonate. S-O vibration positioned at 600 cm^{-1} , 615 cm^{-1} and 677 cm^{-1} was associated with anhydrite. Also, Al-O vibrations at 645 cm^{-1} and 690 cm^{-1} were the characteristic peaks of $C_4A_3\check{S}$ [40–44].

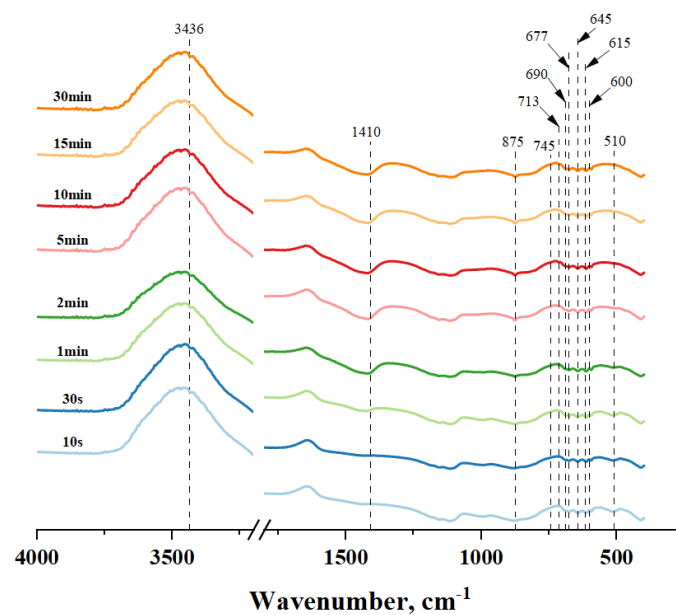


Figure 6. FT-IR curves of the CSA cement carbonation.

3.4. TGA Analysis

The TG-DTG curves of CSA cement at various carbonation times (30 s–30 min) are shown in Figure 7. The main mass loss in the curve between 300 °C and 800 °C was associated with the decomposition of all types of calcium carbonate [43,45,46]. From the result of TG, the calcium carbonate in all of the carbonation samples mainly existed in crystalline morphology, and the amorphous form existed in small amounts, which was consistent with the XRD result. As for the small quantity of mass loss between 50 °C and 150 °C, it was considered the decomposition of gel water or crystal water.

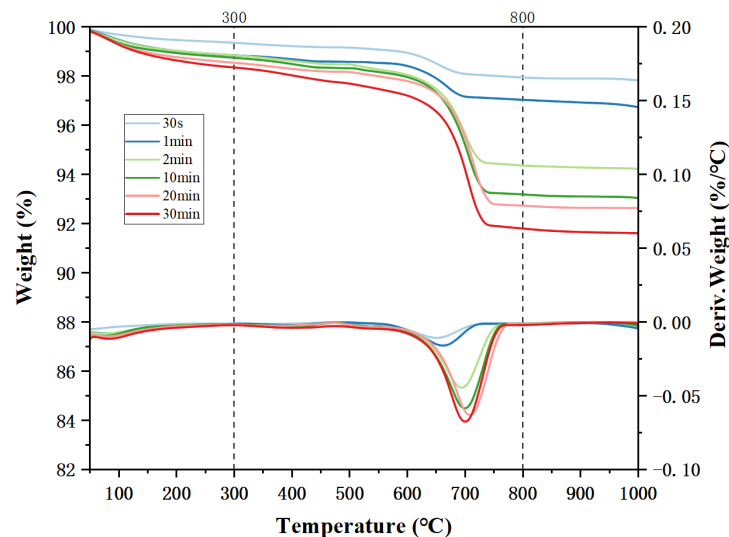


Figure 7. TGA-DTG of various samples after carbonation.

Obviously, with the increase in carbonation time, the content of calcium carbonate increased as well. The detailed mass loss between 300 °C and 800 °C is shown in Figure 8. The samples at the early stage of carbonation (30 s and 1 min) have relatively low mass loss, which illustrates that the carbonation degree was extremely low. The results can also be confirmed by the content of calcium carbonate and amorphous phase in the XRD results. It is obvious that the mass loss increased by 2.68% from 1 min to 2 min after carbonation and

reached 4.49% at 2 min. The total amount of calcium carbonate reached 6.55% at 30 min, which exactly indicated that the carbonation degree was improved as the carbonation time increased.

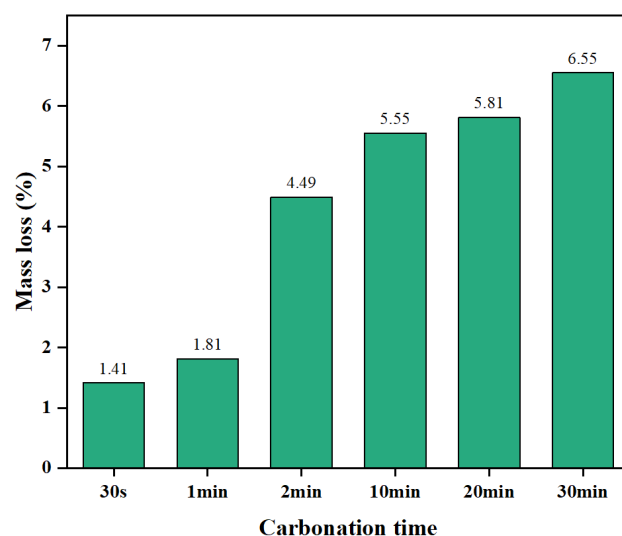


Figure 8. Mass loss between 300 °C and 800 °C of the carbonation samples.

3.5. SEM Analysis

Figure 9 shows the SEM images of the CSA samples at different carbonation times (5 min, 15 min, 30 min). From Figure 9(a-1), the square crystals along with a few needles were observed, which were related to the specific morphology of calcite and aragonite, respectively. Also, the hydration products covered the surface of the cement particles, and the carbonation products, including calcium carbonate crystals and some amorphous gels, were wrapped together (Figure 9(a-2)). When carbonated for 15 min, some agglomerated lamellas were visible, which was associated with the typical morphology of aluminum hydroxide (Figure 9(b-1)). In addition, the silica gel shape was found and formed a network, and the square calcite crystals could be observed with a larger particle size. The vaterite with a typically spherical morphology and the aragonite with the needle-like morphology were visible as well (Figure 9(b-2)). In the sample carbonated for 30 min, its surface was mostly covered by the square calcite crystals, bonding with some silica gel and aluminum hydroxide gel (Figure 9(c-1)). Different from the samples carbonated for 5 min and 15 min, the square calcite crystals were stacked and closed together when carbonated for 30 min, confirming the increasing amount of calcite obtained with the QXRD results (Figure 9(c-2)).

Figure 10 shows the SEM images of the sample carbonated for 1 h and 2 h. The square calcite crystals and spherical vaterite crystals can be observed in Figure 10a, and they gathered on the surface of the unhydrated cement paste. Also, as observed in Figure 10b, a small pore was formed due to the hydration reaction, and the generated calcite crystals not only covered the surface of the unhydrated particles but also filled in the pores. This further revealed that the particles, which should have grown inside the pores, were carbonated directly inside the pore, and calcium carbonate was generated as a result. Furthermore, there were still unhydrated particles existing when carbonated for 1 h and 2 h, and this phenomenon was probably associated with $C_4A_3\check{S}$ in the cement. At the later age of wet carbonation, calcite was the predominant species with a clear contour and a better crystallization, and the morphology no longer changed with the increase in CO_2 . During the early stage, the particle size of calcium carbonate gradually enlarged and piled up; nevertheless, the morphology of the products no longer changed, owing to the abundant calcite generated later.

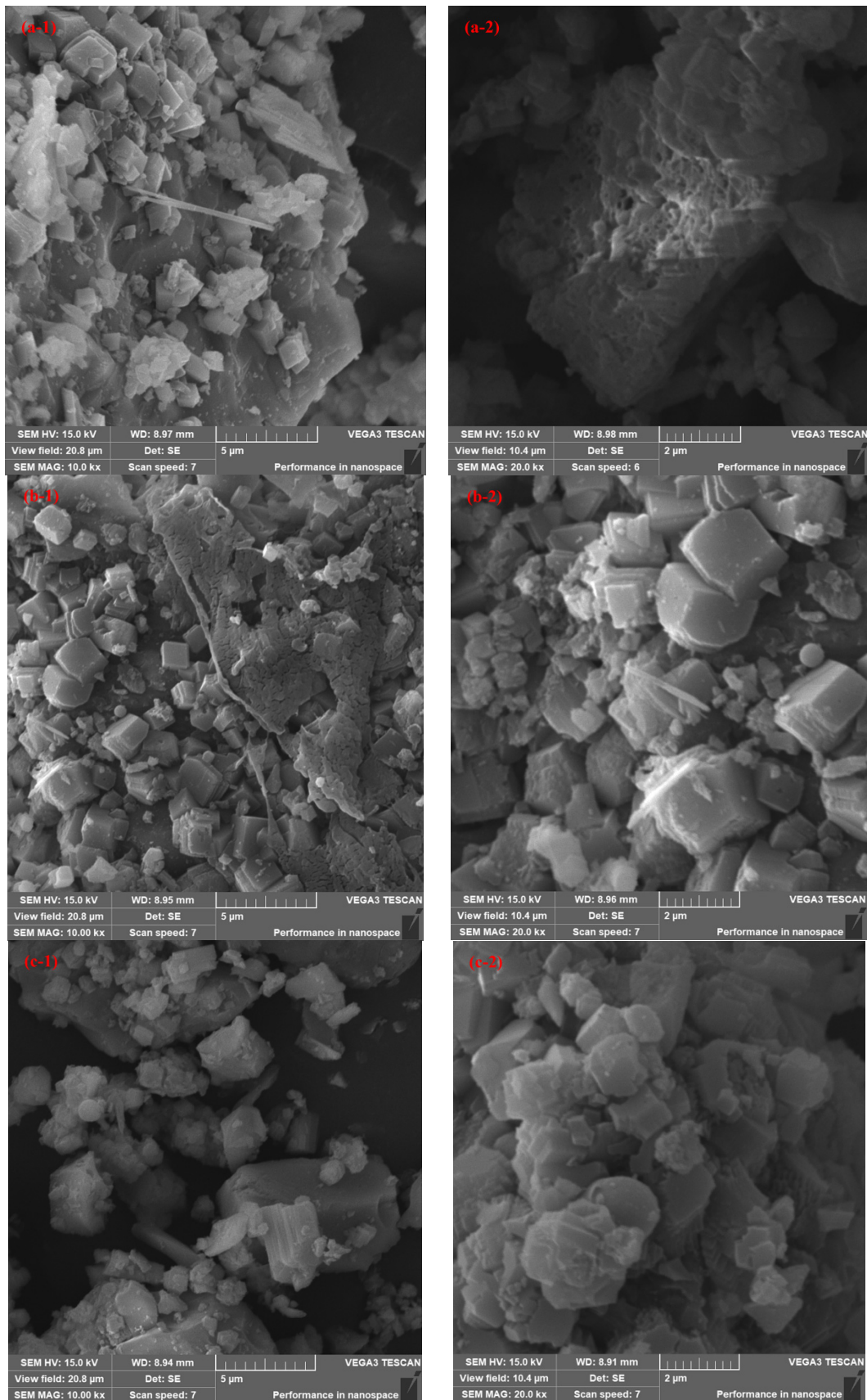


Figure 9. SEM images of the CSA cement carbonated for 5 min (a-1,a-2), 15 min (b-1,b-2) and 30 min (c-1,c-2).

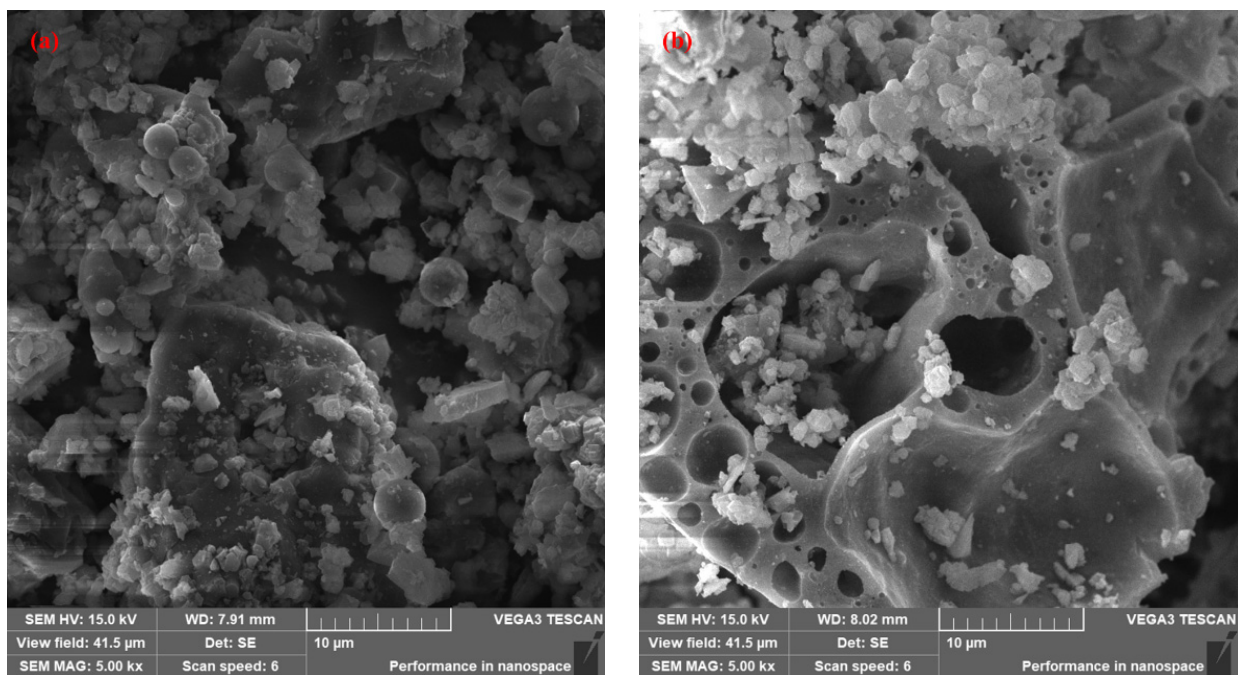
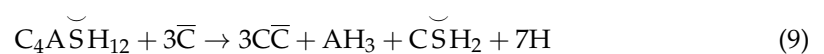
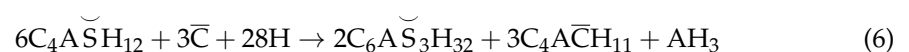


Figure 10. SEM images of the CSA cement carbonated for (a) 1 h and (b) 2 h.

3.6. GEMS Analysis

The modeling method was conducted based on the hydration of CSA cement first and then exposure to CO_2 . The thermodynamic modeling results are demonstrated in Figure 11. It can be observed that, when exposed to CO_2 , the amounts of strätlingite and ettringite began to diminish, and carbon–ettringite was formed as one of the carbonation products of ettringite. As for the existence of strätlingite, it was considered that it was generated from the reaction of C_2S and aluminum hydroxide, which was one of the hydration products of $\text{C}_4\text{A}_3\check{\text{S}}$. With the increasing amount of CO_2 , C_2S was gradually carbonated, and thus, it no longer reacted with aluminum hydroxide. It is worth noting that the thermodynamic modeling of CSA cement carbonation showed the occurrence of mono-carbonate ($\text{C}_4\text{A}\check{\text{C}}\text{H}_{11}$), which was one of the carbonation products of monosulfate. It can be attributed to the carbonation of a small amount of monosulfate generated from the hydration products of $\text{C}_4\text{A}_3\check{\text{S}}$ and water. As is reported by Hargis, the carbonation of monosulfate occurred according to Equations (6)–(9), and when a small amount of CO_2 was added, monosulfate was carbonated according to Equation (6) to generate monocarbonate and ettringite. As an intermediate carbonation product of ettringite, carbon–ettringite only existed under the circumstance of CO_2 ranging from 1 g to 9 g. With the content of ettringite diminished, gypsum, calcium carbonate and aluminum hydroxide were generated as the ultimate carbonation products when CO_2 was abundant [47].



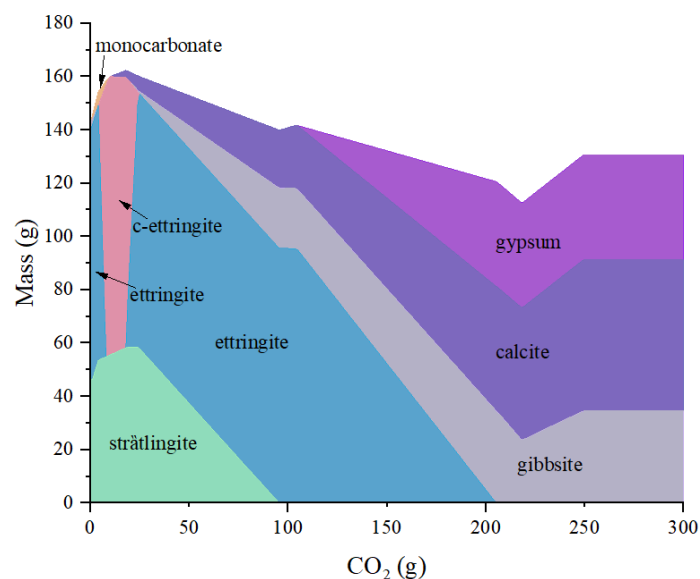


Figure 11. Thermodynamic modeling of the carbonation of CSA cement used in this work.

4. Conclusions

In this work, wet carbonation was used in CSA cement, and the corresponding microstructural evolution was investigated. The conclusions are as follows:

- (1) The pH value changed, showing an increased trend first and a rapid decrease later owing to the carbonation reaction. The slight increase in pH revealed the coupling interaction of the hydration and carbonation reactions in the solution. Ultimately, the pH of the solution was constantly below 7.
- (2) Ettringite, as a main hydration product of $C_4A_3\check{S}$, was not detected throughout the entire carbonation process. This was probably attributed to its immediate carbonation in the solution once formed. The carbonation of ettringite led to the generation of gypsum that would react with $C_4A_3\check{S}$. Consequently, the presence of gypsum was sourced from two parts: One was a composition of CSA cement, and the other was a carbonation product of ettringite.
- (3) The main carbonation product was calcium carbonate, either from the carbonation of ettringite or the hydration product of C_2S . At an early carbonation time, calcite would not generate, and aragonite and vaterite existed predominantly. After 5 min, calcite was generated and showed an obvious increase in number. Furthermore, with the increasing carbonation time, the content of calcium carbonate increased dramatically until C_2S was completely carbonated.
- (4) After carbonation for 24 h, $C_4A_3\check{S}$ still existed in the solution, and C_2S was entirely consumed, which further confirmed that C_2S was easier to be carbonated.
- (5) Thermodynamic modeling of CSA cement further suggested the carbonation of ettringite, and the generation of carbon–ettringite was likely to occur. Also, a small amount of monosulfate probably existed after hydration, and the carbonation of monosulfate would lead to the generation of monocarbonate. The final carbonation products mainly included gypsum, aluminum hydroxide and calcium carbonate.

Author Contributions: Conceptualization, Y.Z., H.Y. and P.S.; methodology, H.Y. and Q.Q.; validation, Q.Z.; formal analysis, C.Z.; resources, Y.Z., Q.Q. and C.Z.; writing—original draft, Y.Z. and H.Y.; writing—review & editing, Y.Z., Q.Z., K.W. and P.S.; supervision, Y.Z., K.W. and P.S. All authors have read and agreed to the published version of the manuscript.

Funding: This work is supported by the National Natural Science Foundation of China (52108252), Science Research Project of Hebei Education Department (BJK2023023), Hebei Natural Science Foundation (E2021203147), Hebei Returned Overseas Chinese Talents Foundation (C20230330), and Key

Laboratory of Advanced Civil Engineering Materials (Tongji University), Ministry of Education (No. 202305).

Data Availability Statement: Data are contained within the article.

Conflicts of Interest: Authors Yangyang Zhang, Quan Qian and Chengwei Zhang were employed by the company Qinhuangdao Municipal Building Materials Group Co., Ltd. The remaining authors declare that the research was conducted in the absence of any commercial or financial relationships that could be construed as a potential conflict of interest.

References

1. Shen, L.; Gao, T.; Zhao, J.; Wang, L.; Liu, L.; Chen, F.; Xue, J. Factory-level measurements on CO₂ emission factors of cement production in China. *Renew. Sustain. Energy Rev.* **2014**, *34*, 337–349. [[CrossRef](#)]
2. Habert, G.; Miller, S.A.; John, V.M.; Provis, J.L.; Favier, A.; Horvath, A.; Scrivener, K.L. Environmental impacts and decarbonization strategies in the cement and concrete industries. *Nat. Rev. Earth Environ.* **2020**, *1*, 559–573. [[CrossRef](#)]
3. Habert, G. Environmental impact of Portland cement production. In *Eco-Efficient Concrete*; Woodhead Publishing: Sawston, UK, 2013; pp. 3–25.
4. Monteiro, N.B.R.; Moita Neto, J.M.; da Silva, E.A. Environmental assessment in concrete industries. *J. Clean. Prod.* **2021**, *327*, 129516. [[CrossRef](#)]
5. Li, Q.; Chen, Z.A.; Zhang, J.T.; Liu, L.C.; Li, X.C.; Jia, L. Positioning and revision of CCUS technology development in China. *Int. J. Greenh. Gas Control* **2016**, *46*, 282–293. [[CrossRef](#)]
6. Plaza, M.G.; Martínez, S.; Rubiera, F. CO₂ Capture, Use, and Storage in the Cement Industry: State of the Art and Expectations. *Energies* **2020**, *13*, 5692. [[CrossRef](#)]
7. Hargis, C.W.; Chen, I.A.; Devenney, M.; Fernandez, M.J.; Gilliam, R.J.; Thatcher, R.P. Calcium Carbonate Cement: A Carbon Capture, Utilization, and Storage (CCUS) Technique. *Materials* **2021**, *14*, 2709. [[CrossRef](#)]
8. Monteiro, J.; Roussanaly, S. CCUS scenarios for the cement industry: Is CO₂ utilization feasible? *J. CO₂ Util.* **2022**, *61*, 102015. [[CrossRef](#)]
9. Shi, C.; Jiménez, A.F.; Palomo, A. New cements for the 21st century: The pursuit of an alternative to Portland cement. *Cem. Concr. Res.* **2011**, *41*, 750–763. [[CrossRef](#)]
10. Hanein, T.; Galvez-Martos, J.-L.; Bannerman, M.N. Carbon footprint of calcium sulfoaluminate clinker production. *J. Clean. Prod.* **2018**, *172*, 2278–2287. [[CrossRef](#)]
11. Tao, Y.; Rahul, A.V.; Mohan, M.K.; De Schutter, G.; Van Tittelboom, K. Recent progress and technical challenges in using calcium sulfoaluminate (CSA) cement. *Cem. Concr. Compos.* **2023**, *137*, 104908. [[CrossRef](#)]
12. Glasser, F.P.; Zhang, L. High-performance cement matrices based on calcium sulfoaluminate–belite compositions. *Cem. Concr. Res.* **2001**, *31*, 1881–1886. [[CrossRef](#)]
13. Naik, T.P. Sustainability of concrete construction. *Pract. Period. Struct. Des. Constr.* **2008**, *13*, 98–103. [[CrossRef](#)]
14. Mo, F.; Li, B.; Li, M.; Fang, Z.; Fang, S.; Jiang, H. Rapid-Hardening and High-Strength Steel-Fiber-Reinforced Concrete: Effects of Curing Ages and Strain Rates on Compressive Performance. *Materials* **2023**, *16*, 4947. [[CrossRef](#)] [[PubMed](#)]
15. Zhang, L.; Glasser, F.P. Investigation of the microstructure and carbonation of CSA-based concretes removed from service. *Cem. Concr. Res.* **2005**, *35*, 2252–2260. [[CrossRef](#)]
16. Hargis, C.W.; Lothenbach, B.; Müller, C.J.; Winnefeld, F. Carbonation of calcium sulfoaluminate mortars. *Cem. Concr. Compos.* **2017**, *80*, 123–134. [[CrossRef](#)]
17. Ansari, W.S.; Chang, J.; ur Rehman, Z.U.; Nawaz, U.; Junaid, M.F. A novel approach to improve carbonation resistance of Calcium Sulfoaluminate cement by assimilating fine cement-sand mix. *Constr. Build. Mater.* **2022**, *317*, 125598. [[CrossRef](#)]
18. Sharma, R.; Kim, H.; Lee, N.K.; Park, J.-J.; Jang, J.G. Microstructural characteristics and CO₂ uptake of calcium sulfoaluminate cement by carbonation curing at different water-to-cement ratios. *Cem. Concr. Res.* **2023**, *163*, 107012. [[CrossRef](#)]
19. Gastaldi, D.; Bertola, F.; Canonico, F.; Buzzi, L.; Mutke, S.; Irico, S.; Paul, G.; Marchese, L.; Boccaleri, E. A chemical/mineralogical investigation of the behavior of sulfoaluminate binders submitted to accelerated carbonation. *Cem. Concr. Res.* **2018**, *109*, 30–41. [[CrossRef](#)]
20. Seo, J.; Yoon, H.N.; Kim, S.; Wang, Z.; Kil, T.; Lee, H.K. Characterization of reactive MgO-modified calcium sulfoaluminate cements upon carbonation. *Cem. Concr. Res.* **2021**, *146*, 106484. [[CrossRef](#)]
21. Bertola, F.; Gastaldi, D.; Irico, S.; Paul, G.; Canonico, F. Influence of the amount of calcium sulfate on physical/mineralogical properties and carbonation resistance of CSA-based cements. *Cem. Concr. Res.* **2022**, *151*, 106634. [[CrossRef](#)]
22. Mechling, J.-M.; Lecomte, A.; Roux, A.; Le Rolland, B. Sulfoaluminate cement behaviours in carbon dioxide, warm and moist environments. *Adv. Cem. Res.* **2014**, *26*, 52–61. [[CrossRef](#)]
23. Seo, J.; Kim, S.; Park, S.; Yoon, H.N.; Lee, H.-K. Carbonation of calcium sulfoaluminate cement blended with blast furnace slag. *Cem. Concr. Compos.* **2021**, *118*, 103918. [[CrossRef](#)]
24. Ho, H.-J.; Iizuka, A.; Shibata, E.; Tomita, H.; Takano, K.; Endo, T. CO₂ Utilization via Direct Aqueous Carbonation of Synthesized Concrete Fines under Atmospheric Pressure. *ACS Omega* **2020**, *5*, 15877–15890. [[CrossRef](#)]

25. Ben Ghacham, A.; Pasquier, L.-C.; Cecchi, E.; Blais, J.-F.; Mercier, G. Valorization of waste concrete through CO₂ mineral carbonation: Optimizing parameters and improving reactivity using concrete separation. *J. Clean. Prod.* **2017**, *166*, 869–878. [[CrossRef](#)]
26. Fang, X.; Xuan, D.; Shen, P.; Poon, C.S. Fast enhancement of recycled fine aggregates properties by wet carbonation. *J. Clean. Prod.* **2021**, *313*, 127867. [[CrossRef](#)]
27. Shen, P.; Zhang, Y.; Jiang, Y.; Zhan, B.; Lu, J.; Zhang, S.; Xuan, D.; Poon, C.S. Phase assemblance evolution during wet carbonation of recycled concrete fines. *Cem. Concr. Res.* **2022**, *154*, 106733. [[CrossRef](#)]
28. Scrivener, K.; Snellings, R.; Lothenbach, B. (Eds.) *A Practical Guide to Microstructural Analysis of Cementitious Materials*; CRC Press: Boca Raton, FL, USA, 2018.
29. Zhang, Y.; Zhao, Q.; Gao, Z.; Chang, J. Nanostructural evolution of Al(OH)₃ gel formed by the cubic and orthorhombic ye'elimite clinkers of calcium sulfoaluminate cements in an ultra-wide hydration temperature range. *Cem. Concr. Res.* **2021**, *150*, 106607. [[CrossRef](#)]
30. Wang, D.; Fang, Y.; Zhang, Y.; Chang, J. Changes in mineral composition, growth of calcite crystal, and promotion of physico-chemical properties induced by carbonation of β-C₂S. *J. CO₂ Util.* **2019**, *34*, 149–162. [[CrossRef](#)]
31. Li, H.; Liu, Y.; Lu, J.; Zhao, W.; Moeen, M.; Guan, X.; Zhu, J. Role of the structure of synthetic Al(OH)₃ on the properties of sulfoaluminate cement-based materials. *Cem. Concr. Res.* **2023**, *174*, 107330. [[CrossRef](#)]
32. Jiang, T.; Cui, K.; Chang, J. Development of low-carbon cement: Carbonation of compounded C₂S by β-C₂S and γ-C₂S. *Cem. Concr. Compos.* **2023**, *139*, 105071. [[CrossRef](#)]
33. Zajac, M.; Skocek, J.; Bullerjahn, F.; Haha, M.B. Effect of retarders on the early hydration of calcium-sulpho-aluminate (CSA) type cements. *Cem. Concr. Res.* **2016**, *84*, 62–75. [[CrossRef](#)]
34. Seo, J.; Kim, S.; Yoon, H.N.; Lee, H.K. Effect of the molar ratio of calcium sulfate over ye'elimite on the reaction of CSA cement/slag blends under an accelerated carbonation condition. *J. Build. Eng.* **2022**, *46*, 103785. [[CrossRef](#)]
35. Song, F.; Yu, Z.; Yang, F.; Liu, Y.; Lu, Y. Strätlingite and calcium hemicarboaluminate hydrate in belite-calcium sulfoaluminate cement. *Ceram. Silik.* **2014**, *58*, 269–274.
36. Singh, N. Hydrothermal synthesis of β-dicalcium silicate (β-Ca₂SiO₄). *Prog. Cryst. Growth Charact. Mater.* **2006**, *52*, 77–83. [[CrossRef](#)]
37. Zhang, Y.; Chang, J.; Ji, J. AH₃ phase in the hydration product system of AFt-AFm-AH₃ in calcium sulfoaluminate cements: A microstructural study. *Constr. Build. Mater.* **2018**, *167*, 587–596. [[CrossRef](#)]
38. Wang, X.; Pan, Z.; Shen, X.; Liu, W. Stability and decomposition mechanism of ettringite in presence of ammonium sulfate solution. *Constr. Build. Mater.* **2016**, *124*, 786–793. [[CrossRef](#)]
39. Kim, H.; Pei, J.; Siddique, S.; Jang, J. Effects of the curing conditions on the carbonation curing efficiency of ordinary Portland cement and a belite-rich cement mortar. *Sustainability* **2021**, *13*, 5175. [[CrossRef](#)]
40. Dos Santos, V.H.J.M.; Pontin, D.; Ponzi, G.G.D.; e Stepanha, A.S.D.G.; Martel, R.B.; Schütz, M.K.; Einloft, S.M.O.; Dalla, F. Application of Fourier Transform infrared spectroscopy (FTIR) coupled with multivariate regression for calcium carbonate (CaCO₃) quantification in cement. *Constr. Build. Mater.* **2021**, *313*, 125413. [[CrossRef](#)]
41. Timón, V.; Torrens-Martin, D.; Fernández-Carrasco, L.J.; Martínez-Ramírez, S. Infrared and Raman vibrational modelling of β-C₂S and C₃S compounds. *Cem. Concr. Res.* **2023**, *169*, 107162. [[CrossRef](#)]
42. Hughes, T.L.; Methven, C.M.; Jones, T.G.; Pelham, S.E.; Fletcher, P.; Hall, C. Determining cement composition by Fourier transform infrared spectroscopy. *Adv. Cem. Based Mater.* **1995**, *2*, 91–104. [[CrossRef](#)]
43. Chang, J.; Jiang, T.; Cui, K. Influence on compressive strength and CO₂ capture after accelerated carbonation of combination β-C₂S with γ-C₂S. *Constr. Build. Mater.* **2021**, *312*, 125359. [[CrossRef](#)]
44. Torrén-Martín, D.; Fernández-Carrasco, L.; Martínez-Ramírez, S. Hydration of calcium aluminates and calcium sulfoaluminate studied by Raman spectroscopy. *Cem. Concr. Res.* **2013**, *47*, 43–50. [[CrossRef](#)]
45. Chang, X.; Liu, S.; Zhang, C.; Shen, P.; Xuan, D.; Guan, X.; Shi, C. Carbonation-hardening properties and ITZ microstructure of low-calcium CO₂ sequestration binder mortar. *Constr. Build. Mater.* **2022**, *336*, 127589. [[CrossRef](#)]
46. Chang, J.; Fang, Y. Quantitative analysis of accelerated carbonation products of the synthetic calcium silicate hydrate (C-S-H) by QXRD and TG/MS. *J. Therm. Anal. Calorim.* **2015**, *119*, 57–62. [[CrossRef](#)]
47. Pelletier, L.; Winnefeld, F.; Lothenbach, B. The ternary system Portland cement–calcium sulfoaluminate clinker–anhydrite: Hydration mechanism and mortar properties. *Cem. Concr. Compos.* **2010**, *32*, 497–507. [[CrossRef](#)]

Disclaimer/Publisher's Note: The statements, opinions and data contained in all publications are solely those of the individual author(s) and contributor(s) and not of MDPI and/or the editor(s). MDPI and/or the editor(s) disclaim responsibility for any injury to people or property resulting from any ideas, methods, instructions or products referred to in the content.